J. Fluid Mech. (2006), *vol.* 568, *pp.* 273–301.
doi:10.1017/S0022112006002485 Printed in the United Kingdom

On radiating solitons in a model of the internal wave–shear flow resonance

By VYACHESLAV V. VORONOVICH[1]†
IGOR A. SAZONOV[2]‡ AND VICTOR I. SHRIRA[3]

[1]Department of Applied Mathematics, University College Cork, Ireland
[2]Civil & Computational Engineering Centre, University of Wales Swansea, SA2 8PP UK
[3]Department of Mathematics, Keele University, Keele, ST5 5BG UK

(Received 30 July 2003 and in revised form 5 May 2006)

The work concerns the nonlinear dynamics of oceanic internal waves in resonance with a surface shear current. The resonance occurs when the celerity of the wave matches the mean flow speed at the surface. The evolution of weakly nonlinear waves long compared to the thickness of the upper mixed layer is found to be described by two linearly coupled equations (a linearized intermediate long wave equation and the Riemann wave equation). The presence of a pseudodifferential operator leads to qualitatively new features of the wave dynamics compared to the previously studied case of shallow water. The system is investigated primarily by means of numerical analysis. It possesses a variety of both periodic and solitary wave stationary solutions, including 'delocalized solitons' with a localized core and very small non-decaying oscillatory tails (throughout the paper we use the term 'soliton' as synonymous with 'solitary wave' and do not imply any integrability of the system). These 'solitons' are in linear resonance with infinitesimal waves, which in the evolutionary problem normally results in radiative damping. However, the rate of the energy losses proves to be so small, that these delocalized radiating solitons can be treated as quasi-stationary, that is, effectively, as true solitons at the characteristic time scales of the system. Moreover, they represent a very important class of intermediate asymptotics in the evolution of initial localized pulses. A typical pulse evolves into a sequence of solitary waves of all kinds, including the 'delocalized' ones, plus a decaying train of periodic waves. The remarkable feature of this evolution is that of all the products of the pulse fission (in a wide range of parameters of the initial pulse) the radiating solitons have by far the largest amplitudes. We argue that the radiating solitons acting as intermediate asymptotics of initial-value problems are a generic phenomenon not confined to the particular model under consideration.

1. Introduction

Manifestations of the internal waves on the ocean surface have long attracted the attention of both observationally and theoretically minded oceanographers. Numerous field experiments have been conducted and extensive databases of *in situ*

† Permanent address: P. P. Shirshov Institute of Oceanology RAS, 36 Nakhimovsky pr., 117851 Moscow, Russia.
‡ Permanent address: A. M. Obuhov Institute of Atmospheric Physics RAS, 2 Phyzhevskii per., 119017 Moscow, Russia.

measurements of internal waves in both the bulk of the ocean and in the upper mixed layer are now available (e.g. IOS/WHOI/ONR 1999). Continuing progress in remote sensing of the ocean surface, in turn, has provided numerous satellite images of the typical signatures caused by internal waves (see e.g. Klemas, Zheng & Yan 1998).The interest in the interplay of complicated physical mechanisms leading to such manifestations has resulted in vast literature; however, the basics are quite simple and straightforward. A propagating internal wave creates an inhomogeneous surface velocity field, i.e areas of the few convergency and divergence at the surface, which results in considerable changes in observable properties of the ocean surface, such as albedo, breaking patterns of short gravity waves (and therefore, the cross-section of microwave scattering), floating seaweed and ice distribution.

Hence, patterns of intermittent stripes of floating material or areas with higher and lower albedo (slicks) are routinely observed when internal waves are present. Surprisingly, slicks at the water surface have been reported even when no internal waves were detected by the standard techniques at the thermocline depth (A. N. Serebryany 2002, personal communication). A possible interpretation of such observations is that under certain conditions, even quite weak internal waves can produce significant surface signatures. A model based upon this line of thought aimed at explaining this phenomenon was proposed by Voronovich & Shrira (1996), who assumed the internal wave-shear flow resonance to be the underlying mechanism. The resonance occurs when there is a surface current strong enough for its velocity at the surface to coincide with the celerity of an internal wave propagating in the bulk of the ocean. It results in an order of magnitude amplification of the wave-induced horizontal velocity field at the surface and, thus, makes the surface signatures of even comparatively weak internal waves pronounced and easily detectable.

A nonlinear model of the resonance in shallow water was developed later by Voronovich, Pelinovsky & Shrira (1998*a*), who employed the concept of a *vorticity wave* to describe the flow perturbations (see Shrira 1989), and derived a system of coupled evolution equations for the wave amplitudes. The system possesses both periodic and solitary wave solutions belonging to the two different families, which move respectively slightly faster and slower than the linear waves. The amplitude of the 'fast' waves is limited from above by a *peaked soliton*, i.e. a solitary wave with a sharp corner at the crest. Numerical simulations showed that the solitary waves represent 'attractors' for the 'subcritical' localized pulses, i.e. with initial amplitudes below a certain threshold, which evolve into a sequence of solitary waves plus an oscillatory tail. 'Supercritical' pulses develop vertical slopes at the front in finite time, which indicates wave breaking. The properties of the system and of the solitary waves, in particular, were found to depend heavily on the value of the mismatch in the phase speeds of the interacting waves, the only external parameter in the system. When an internal wave travels over a variable depth, e.g. through the shelf region, its celerity evolves and so does the mismatch. Shrira, Voronovich & Sazonov (2000) studied the dynamics of the resonant waves over a sloping bottom and showed that both periodic and solitary waves propagating onshore grow in amplitude, eventually reach the limiting configuration, and then break. The breaking occurs mainly in the upper layer whereas the motion at depth remains smooth. Breaking events may represent an important mechanism of a poorly accounted for contribution of the internal waves to the mixing processes in the upper layer, which have a profound impact on the energy, momentum, mass and heat exchange between the ocean and the atmosphere.

The aforementioned studies were concerned with the shallow-water approximation, restricting the applicability of the model to the regions of continental shelves and

shallow seas and lakes. Nevertheless, the resonance can occur in the deep and intermediate ocean as well, provided certain conditions are met. The study of the resonant interaction between internal waves and a surface current in deep and finite-depth water represents the primary subject of this paper. In § 2 by means of an asymptotic analysis we derive a set of coupled evolution equations governing the resonance between the current and internal waves long compared to the thickness of the upper mixed layer:

$$a_t + 2aa_x - b_x = 0, \tag{1.1a}$$

$$b_t + \delta b_x - \tilde{\mathscr{L}}[b_x] - a_x = 0. \tag{1.1b}$$

The dispersion in (1.1) is described by an integral operator $\tilde{\mathscr{L}}$, with the kernel dependent on the depth. The study of nonlinear waves governed by non-local equations represents a special challenge: there is no regular technique and very little intuition based on accumulated previous experience. Equations (1.1) possesses a number of integrals of motion corresponding to the 'mass', 'momentum' and the 'energy' of the wave field, which are discussed in § 3. There exist two types of infinitesimal harmonic solutions, with the spectrum of velocities limited from above and separated by a gap (forbidden zone).

Stationary solitary waves are studied numerically in § 4. They exist in the gaps of the linear spectrum, with their speed limited from above. The limiting wave has a sharp corner at the crest, which corresponds to the nonlinear critical layer formed as the speed of the particles swept by the wave attains the wave phase speed. Apart from the common 'gap' solitons, so-called 'delocalized' ones characterized by two symmetric infinite oscillatory tails were found in the range of propagation speeds belonging to the linear wave spectrum. In the evolutionary setting these objects, on the one hand, are obviously non-stationary, as the resonance with infinitesimal waves leads to radiative damping; on the other hand, the rate of energy loss proves to be extremely small, which allows one to treat them as if they were true stationary waves. Numerical results are partially corroborated by an asymptotic analysis of the radiation. In § 5 the evolution of the localized pulses within the framework of (1.1) is studied numerically. 'Subcritical' pulses, i.e. those for which the values of the integrals of motion do not exceed a certain threshold, evolve into a sequence of solitary waves, with the 'delocalized' ones having by far the largest amplitudes in the sequence. 'Supercritical' pulses develop a vertical slope at the front and, eventually, break. The results, their implications and the wider context are briefly discussed in the conclusive § 6.

2. The model, scaling and asymptotic analysis

2.1. *The model and basic assumptions*

We study the dynamics of long waves in an inviscid and incompressible fluid in the presence of a surface shear current. The x-axis of the coordinate frame is in the direction of the current and z is vertically upward. For the sake of simplicity we consider the simplest model, based on the following assumptions:

(i) The fluid consists of two homogeneous layers separated at $z = -H$ by a density jump $\Delta\rho = \rho_2 - \rho_1 > 0$ which is assumed to be small:

$$\Delta\rho/\rho_{1,2} \ll 1. \tag{2.1a}$$

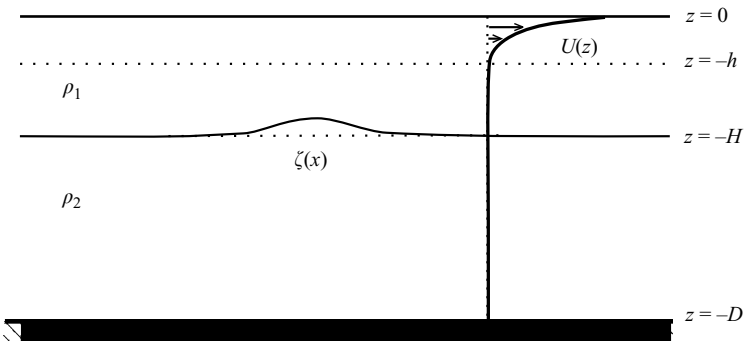

FIGURE 1. Geometry and notation.

(ii) The density interface depth H is small compared to the total depth D:

$$H/D \ll 1. \tag{2.1b}$$

(iii) The current is assumed to be planar $\boldsymbol{U} = \{U(z), 0, 0\}$ and to occupy only a small fraction of the upper layer $-h < z < 0$:

$$h/H \ll 1. \tag{2.1c}$$

(iv) Velocity U and its gradient decrease monotonically with z and are negligibly small below $-h$ (see figure 1).
(v) For the sake of simplicity, the spanwise motions and variations are neglected.
(vi) The study is restricted to long wave perturbations with the characteristic horizontal scale (wavelength) λ such that

$$H/\lambda \ll 1. \tag{2.1d}$$

2.2. *Governing equations and boundary conditions*

In the presence of parallel mean flow $\boldsymbol{U}(z)$ the motion of inviscid incompressible fluid can be described by the following set of equations:

$$(\partial_t + U\partial_x)\nabla^2 w - U_{zz} w_x = (uu_x + wu_z)_{xz} - (uw_x + ww_z)_{xx}, \tag{2.2a}$$

$$u_x + w_z = 0, \tag{2.2b}$$

where $u(t, x, z)$, $w(t, x, z)$ are the horizontal and vertical velocity perturbations about the mean flow. Subscripts denote the corresponding derivatives.

Solutions of (2.2) must satisfy the 'rigid lid' condition (see e.g. Leblond & Mysak 1979) at the surface and the non-permeability condition at the bottom, presumed to be flat:

$$w = 0 \quad \text{at } z = 0 \text{ and } z = -D. \tag{2.3}$$

The fluid consists of three layers: the uppermost, of light fluid, occupied by the current; the middle, of the same light fluid, but without a current; and the lower, of heavier fluid without currents. Solutions of (2.2) in each of them must be matched at the interfaces: the interface displacement and pressure have to be continuous. At the upper interface there is a jump in neither density nor vorticity, hence the velocity field is continuous. This implies

$$[w] = 0, \quad [w_z] = 0 \quad \text{at} \quad z = -h, \tag{2.4}$$

where $[f]$ denotes a jump in a variable f at the interface. At the lower interface (density jump) (see Appendix A)

$$[u\zeta_x - w] = 0, \tag{2.5a}$$

$$[u_t + uu_x + wu_z] + [w_t + uw_x + ww_z]\zeta_x - g'\zeta_x = 0 \quad \text{at} \quad z = -H + \zeta, \tag{2.5b}$$

where $g' = g\Delta\rho/\rho_1$; $\zeta(t, x)$ is the interface deflection due to the wave perturbation. It can be found from the kinematic condition

$$\zeta_t + u\zeta_x = w \quad \text{at} \quad z = -H + \zeta. \tag{2.6}$$

The system (2.2)–(2.6) constitutes the framework of the analysis to follow.

2.3. *Scaling*

The scales of vertical motion in the three layers, h, H and λ, are different and widely separated. A qualitative preliminary analysis suggests that the 'distinguished limit' is realized (e.g. Nayfeh 1993), that is the largest number of various physical phenomena are taken into account correctly, when these scales satisfy the relation

$$\frac{h}{H} = \left(\frac{H}{\lambda}\right)^2 = \epsilon^2 \ll 1, \tag{2.7}$$

which is assumed to hold hereinafter. Equation (2.7) defines the key small parameter ϵ in our analysis.

Let us introduce the non-dimensional variables (denoted by asterisk)

$$x_* = \frac{x}{\lambda}, \qquad z_* = \frac{z}{\langle z\rangle}, \qquad t_* = \frac{U_0}{\lambda}\,t,$$

$$u = \langle u\rangle\, U_0 u_*, \quad w = \langle w\rangle\, U_0 w_*, \quad \zeta_* = \frac{\zeta}{\langle\zeta\rangle},$$

the scales $\langle\ldots\rangle$ being different in each layer, $U_0 = U(0)$. Note that only $\langle u\rangle$, $\langle z\rangle$ are independent, as the other scales are related to them through (2.2b) and (2.6):

$$\langle w\rangle = \frac{\langle z\rangle}{\lambda}\,\langle u\rangle, \quad \langle\zeta\rangle = \langle u\rangle\langle z\rangle. \tag{2.8}$$

It is convenient to choose a reference frame moving with the celerity of the linear wave $c = U_0\, c_*$, i.e. introduce a running coordinate

$$\chi_* = x_* - c_* t_*. \tag{2.9a}$$

The evolution in such a reference frame occurs on much slower time scale, i.e. for any physical field

$$f(t_*, x_*, z_*) = f(\epsilon\tau, \chi_*, z_*). \tag{2.9b}$$

The non-dimensional version of (2.2) is then (asterisks are dropped)

$$(\epsilon\partial_\tau + \sigma\partial_\chi)\left(w_{zz} + \frac{\langle z\rangle^2}{\lambda^2}w_{\chi\chi}\right) - \sigma_{zz}w_\chi = \langle u\rangle\left[(uu_\chi + wu_z)_z - \frac{\langle z\rangle^2}{\lambda^2}(uw_\chi + ww_z)_\chi\right]_\chi, \tag{2.10a}$$

$$u_\chi + w_z = 0, \tag{2.10b}$$

where $\sigma = U(z) - c$.

2.4. *Asymptotic analysis and evolution equations*

In each of the layers a solution is sought in the form of an asymptotic series in powers of ϵ:

$$\{u, w\} = \sum_{n=0}^{\infty} \epsilon^n \{u_n, w_n\}. \tag{2.11}$$

In the uppermost layer (all variables are marked by a hat)

$$\langle \hat{u} \rangle = \epsilon, \quad \langle \hat{z} \rangle = h, \tag{2.12}$$

and (2.10*a*) becomes

$$(\sigma \hat{w}_{\hat{z}\hat{z}} - \sigma_{\hat{z}\hat{z}} \hat{w})_\chi = \epsilon \hat{w}_{\hat{z}\hat{z}\tau} + \epsilon (u u_\chi + w u_z)_{\hat{z}\chi} + o(\epsilon). \tag{2.13}$$

On substituting (2.11) into (2.13) we obtain

$$\hat{w} = -\sigma A_\chi - \epsilon \left(A_\tau + \sigma_{\hat{z}} A A_\chi + \sigma B_\chi \int^{\hat{z}} \frac{c^2}{\sigma^2} \, \mathrm{d}z' \right) + \cdots, \tag{2.14a}$$

$$\hat{u} = \sigma_{\hat{z}} A + \epsilon \left(\frac{\sigma_{\hat{z}\hat{z}}}{2} A^2 + \frac{c^2}{\sigma} B + \sigma_{\hat{z}} B \int^{\hat{z}} \frac{c^2}{\sigma^2} \, \mathrm{d}z' \right) + \cdots, \tag{2.14b}$$

where $A(\tau, \chi)$ and $B(\tau, \chi)$ are as yet unknown functions specifying amplitudes of the vorticity wave and internal wave, respectively. At the main order the motion of fluid particles in the uppermost layer represents a 'pure' vorticity wave (see Voronovich, Shrira & Stepanyantz 1998*b*), unaffected by the resonant interaction. The effect of the internal wave comes only at the second order of (2.14).

Applying the boundary condition at the surface specifies the value of the phase speed of the vorticity wave:

$$c = U_0 \tag{2.15a}$$

and yields the evolution equation for the wave amplitude:

$$A_\tau + U_0' A A_\chi - \frac{U_0^2}{U_0'} B_\chi = 0, \tag{2.15b}$$

where $U_0' = U_{\hat{z}}(0)$. It should be mentioned that the streamwise velocity component u_1 is divergent,

$$\hat{u}_1 \simeq -B_\chi \frac{U_0''}{U_0'^2} \log |\hat{z}| + \cdots, \quad \hat{z} \to 0. \tag{2.16}$$

This divergence indicates the presence of a critical layer at $\hat{z} = 0$ and, normally, requires special attention. However, the analysis carried out by Voronovich *et al.* (1998*b*) shows that the critical layer contribution to (2.15*b*) is, to the leading order, negligible for two-dimensional motions, which for the time scales we are interested in enables us to ignore it.

In the middle layer (the variables are marked by an overbar)

$$\langle \bar{u} \rangle = \epsilon^2, \quad \langle \bar{z} \rangle = H, \tag{2.17}$$

the current is absent, (2.10*a*) is

$$(-c\bar{w}_\chi + \epsilon \bar{w}_\tau)_{\bar{z}\bar{z}} = o(\epsilon) \tag{2.18}$$

and the vertical velocity dependence on depth is linear. Applying matching conditions (2.4) at $\hat{z} \to -\infty$, $\bar{z} \to 0$, we obtain

$$\bar{w} = c B_\chi \bar{z} + \epsilon (c A_\chi + R_\chi \bar{z}) + \cdots, \tag{2.19a}$$

$$\bar{u} = -cB - \epsilon R + \cdots, \tag{2.19b}$$

where $R(\tau, \chi)$ is a correction to the amplitude of the internal wave; it plays no role in the adopted approximation.

In the bottom layer (the variables are marked by a breve)

$$\langle \breve{u} \rangle = \epsilon^3, \quad \langle \breve{z} \rangle = \lambda. \tag{2.20}$$

The density being constant, the fluid still and the horizontal and vertical scales equal, the motion is potential and (2.2*a*) takes the form

$$\breve{w}_{\breve{z}\breve{z}} + \breve{w}_{\chi\chi} = o(\epsilon^2). \tag{2.21}$$

Its solution is sought as a combination of the primary Fourier harmonics with amplitudes depending on time and depth in terms of a wavetrain amplitude $\Phi(\tau, \chi)$

$$\breve{w} = \mathscr{F}^{-1}\left[\mathscr{F}[\Phi_\chi] \frac{\phi(k, \breve{z})}{\phi(k, 0)} \right] + o(1), \tag{2.22}$$

where $\mathscr{F}$, $\mathscr{F}^{-1}$ stand respectively for the direct and inverse Fourier transforms in χ. The mode function $\phi(k, \breve{z})$ is determined from the boundary problem

$$\phi_{\breve{z}\breve{z}} - k^2\phi = 0, \tag{2.23a}$$

$$\phi(k, \breve{z}) \to 0, \quad \breve{z} \to -D_*, \tag{2.23b}$$

where $D_* = D/\lambda$ is the total non-dimensional depth.

The wavetrain amplitude $\Phi(\tau, \chi)$ is easily found from the matching condition (2.5*a*) at the density jump. From (2.8), the scale of the interface displacement is

$$\langle \zeta \rangle = \epsilon^2 H = \epsilon^3 \lambda.$$

It is so small that the difference between the vertical velocity and that normal to the interface is negligible. Moreover, the values of the wave field components at the moving interface are very well approximated by those at its unperturbed position. Hence, (2.5*a*) transforms into

$$w|_{\hat{z}=-1} = \breve{w}|_{\breve{z}=0} + o(\epsilon), \tag{2.24}$$

which results in

$$\breve{w} = -c\mathscr{F}^{-1}\left[\mathscr{F}[B_\chi] \frac{\phi(k, \breve{z})}{\phi(k, 0)} \right] + o(1), \tag{2.25a}$$

$$\breve{u} = c\mathscr{F}^{-1}\left[\mathscr{F}[B] \frac{\phi_{\breve{z}}}{\phi}\bigg|_{\breve{z}=0} \right] + o(1). \tag{2.25b}$$

2.5. *Matching at the density jump*

The last condition to be satisfied is (2.5*b*). Again, due to the very small amplitude of the interface displacement it can be approximated by

$$\{-cu_\chi + \epsilon(u_t + uu_\chi + wu_{\bar{z}})\}_{\bar{z}=-1} - \left(\frac{c_{in}}{U_0}\right)^2 \zeta_\chi = -\epsilon c\breve{u}_\chi|_{\breve{z}=0} + o(\epsilon). \tag{2.26}$$

Here

$$c_{in} = \sqrt{g'H}$$

is the celerity of the long internal wave travelling at the density interface. In resonance conditions c_{in} must be close, but not necessarily equal, to the current's speed at the

surface, i.e.

$$\frac{\sqrt{g'H}}{U_0} = 1 + \epsilon\,\omega, \tag{2.27}$$

where ω is the difference in the phase speeds of the interacting waves. The interface displacement can be found from the kinematic boundary condition (2.6):

$$\zeta = B + \epsilon\left(-A + \frac{1}{c}\,\partial_\chi^{-1} B_\tau + \frac{1}{c} R\right) + \cdots. \tag{2.28}$$

Finally, substituting (2.19), (2.27) and (2.28) into (2.26) we obtain an evolution equation for the internal wave amplitude $B(\tau, \chi)$:

$$B_\tau + \omega B_\chi - \frac{c}{2}\,\tilde{\mathscr{L}}[B_\chi] - \frac{c}{2}\,A_\chi = 0, \tag{2.29a}$$

where

$$\tilde{\mathscr{L}}[f] = \mathscr{F}^{-1}[\mathscr{F}[f]\,(\phi'/\phi)|_{\check{z}=0}]. \tag{2.29b}$$

Equations (2.15*b*), (2.29) constitute a closed system describing the dynamics of the wave amplitudes at the resonance conditions in deep and finite-depth water. On re-scaling the dependent and independent variables

$$a = 2\gamma^2 A, \qquad b = 2\gamma^3 B, \qquad \delta = \gamma\,\omega, \qquad x = \frac{\chi}{\gamma}, \qquad t = \frac{c}{2\gamma^2}\,\tau, \tag{2.30a}$$

where γ is the coefficient given by

$$\gamma = \left(\frac{U_{\hat{z}}}{2U}\right)^{1/2}_{\hat{z}=0}, \tag{2.30b}$$

the system (2.15*b*), (2.29) reduces to the form

$$a_t + (a^2)_x - b_x = 0, \quad b_t + \delta\, b_x - \tilde{\mathscr{L}}[b_x] - a_x = 0 \tag{2.31}$$

where the only parameter left is δ, the mismatch in the phase velocities of the interacting waves.

Although it is more convenient to deal with the system cast into the simplest form (2.31), it is worth keeping in mind the physical meaning of the dependent variables a and b: b is normalized amplitude of the internal gravity wave mode, more specifically, it can be viewed as the deflection of the density interface; a is normalized amplitude of the vorticity mode in the uppermost layer and can be viewed as the normalized perturbation of the surface velocity.

3. Dispersive properties and conservation laws

To elucidate the expressions for $\tilde{\mathscr{L}}$ consider first a deep fluid, i.e. of depth large compared to a typical wavelength. The solution of (2.23) vanishing at minus infinity is

$$\phi(k, \check{z}) = \exp\{|k|\,\check{z}\}$$

and, hence,

$$\tilde{\mathscr{L}}[f] = \mathscr{F}^{-1}[\mathscr{F}[f]|k|] = -\tilde{\mathscr{H}}\,[f_\chi], \tag{3.1}$$

where $\tilde{\mathscr{H}}$ is the Hilbert transform. In fluid of finite depth, i.e. comparable to the wavelength, the solution of (2.23) is

$$\phi_k(\check{z}) = \sinh\{k(\check{z} + D_*)\},$$

and

$$\tilde{\mathscr{L}}[f] = \mathscr{F}^{-1}[\mathscr{F}[f]k\coth(kD_*)] = -\tilde{\mathscr{J}}[f_\chi], \tag{3.2}$$

where $\tilde{\mathscr{J}}$ is the Joseph operator (Joseph 1977). Note that (3.2) reduces to (3.1) in the deep water limit, i.e. when $D_* \to \infty$.

3.1. *Conservation laws*

The system (2.31) possesses several integrals of motion. The quantities

$$\mathscr{M}[a] = \int_{-\infty}^{\infty} a\,\mathrm{d}x, \qquad \mathscr{M}[b] = \int_{-\infty}^{\infty} b\,\mathrm{d}x. \tag{3.3a}$$

$$\mathscr{P}[a,b] = \frac{1}{2}\int_{-\infty}^{\infty}(a^2+b^2)\,\mathrm{d}x, \tag{3.3b}$$

$$\mathscr{E}[a,b] = \frac{1}{2}\int_{-\infty}^{\infty}\left(\delta\, b^2 + b\,\tilde{\mathscr{G}}[b_x] + \tfrac{2}{3}a^3 - 2ab\right)\mathrm{d}x, \tag{3.3c}$$

are time-independent, provided the functions $a(x,t)$, $b(x,t)$ corresponding to the wave amplitudes are localized, or periodic. In the latter case the integrals in (3.3) must be interpreted as those over the period.

Here $\tilde{\mathscr{G}}$ may represent both Hilbert and Joseph operators, or, in general, any operator connected with (2.29*b*) by the rule

$$\tilde{\mathscr{L}}[f] = -\tilde{\mathscr{G}}[f_x].$$

It is worth noting that (2.31) can be obtained from the constrained variational problem $\delta\Lambda = 0$, where Λ is the Lyapunov functional given by $\Lambda = \mathscr{E} + v\mathscr{P}$ and v serves as a Lagrange multiplier. In other words, the stationary solitary wave solutions can be regarded as extremal points of the functional $\mathscr{E}$ at a fixed value of $\mathscr{P}$. These two conserved quantities are then the 'energy' and the 'momentum' of the nonlinear wave field.

3.2. *Infinitesimal harmonic waves*

It is illuminating to consider first solutions to (2.31) in the small-amplitude limit. Let us look for solutions in the form of a harmonic wave

$$\begin{pmatrix} a \\ b \end{pmatrix} = \begin{pmatrix} \tilde{a} \\ \tilde{b} \end{pmatrix} \exp\{\mathrm{i}k(x - vt)\}, \qquad |\tilde{a}|, |\tilde{b}| \ll 1 \tag{3.4}$$

where k and v are the wavenumber and celerity of the linear wave. Substituting (3.4) into (2.31) and neglecting the nonlinear term we end up with a system of algebraic equations

$$v\tilde{a} + \tilde{b} = 0, \quad \tilde{a} + (v - \delta + Q(k))\tilde{b} = 0 \tag{3.5a, b}$$

where

$$Q(k) = \left.\frac{\phi'}{\phi}\right|_{z=0}$$

is the Fourier transform of the kernel of the operator $\tilde{\mathscr{L}}$. Non-trivial solutions of (3.5) exist only if

$$v = \tfrac{1}{2}\left\{\delta - Q(k) \pm ([\delta - Q(k)]^2 + 4)^{1/2}\right\}. \tag{3.6}$$

Equation (3.6) is the dispersion relation of infinitesimal harmonic waves, a typical example being shown in figure 2. Linear waves belong to two different branches:

$$-\infty < v \leqslant c_- < 0, \qquad 0 \leqslant v \leqslant c_+, \tag{3.7}$$

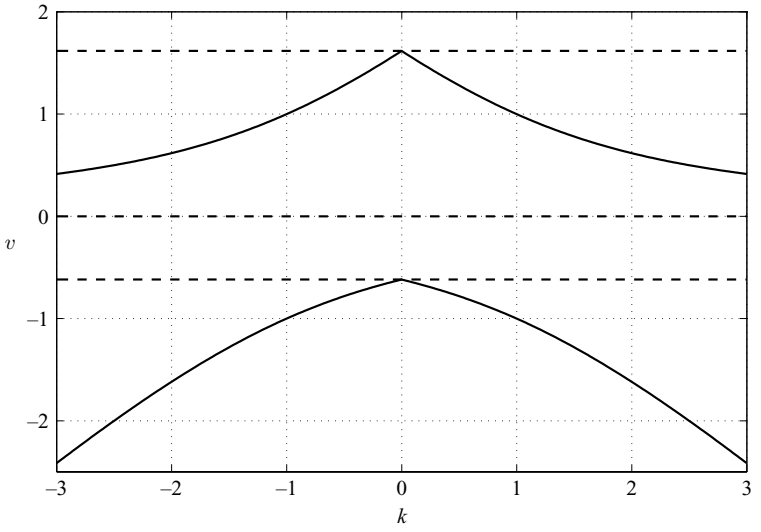

FIGURE 2. An example of the dispersion curve for linear waves (deep water, $\delta = 1$).

which correspond to the vorticity and density interface gravity modes modified by their interaction in the vicinity of the resonance.

The limiting values of the phase velocity $c_\pm$ are specified by the kernel of the dispersion operator: in the deep water limit

$$Q(k) = |k|, \qquad c_\pm = \tfrac{1}{2}\{\delta \pm \sqrt{\delta^2 + 4}\}; \tag{3.8a}$$

in water of finite depth

$$Q(k) = k\coth(kD_*), \qquad c_\pm = \frac{1}{2}\left\{\delta - \frac{1}{D_*} \pm \sqrt{\left(\delta - \frac{1}{D_*}\right)^2 + 4}\right\}. \tag{3.8b}$$

Below we will use short-wave asymptotics ($|Q(k)| \gg 1$) for the upper branch of the dispersion relation (3.6), which implies

$$v \simeq \frac{1}{|Q(k)|} \qquad \left(\text{for deep water} \qquad v \simeq \frac{1}{|k|}\right). \tag{3.9}$$

4. Solitary waves

For any value of δ there exist two gaps in the spectrum of the linear wave speeds. Therefore, one may expect nonlinear solitary waves (gap solitons) to travel with the velocities lying inside the forbidden zones (see e.g. de Sterke & Sipe 1994). With this in mind, we look for stationary solutions preserving their form and advancing with a constant speed:

$$a = a_s(\xi), \quad b = b_s(\xi), \quad \text{where} \quad \xi = x - vt, \tag{4.1}$$

with the analysis centred on solitary waves, such that $a_s, b_s \to 0$ as $x \to \pm\infty$ (it would also be of interest to investigate kink solitons but this goes beyond the scope of the present paper). On substituting (4.1) into (2.31) and integrating it once with respect to ξ we obtain

$$a_s^2 - va_s - b_s = 0, \quad (v - \delta + \tilde{\mathscr{L}})b_s + a_s = 0 \tag{4.2a, b}$$

Equations (4.2) do not allow one to use the phase-plane analysis successfully employed by Voronovich *et al.* (1998*a*) to treat a similar problem in shallow water. The non-local pseudo-differential dispersion operators $\tilde{\mathscr{L}}$ encountered both in deep and finite-depth water result in the phase space of the system having an infinite number of dimensions. So far, no non-trivial analytical solutions have been found. Instead we have to resort to numerics, the details of which can be found in Appendix B. The numerics yields solitary waves with v lying in the gaps of the linear spectrum

$$v \in (c_-; \min\{\delta, 0\}), \qquad \text{gap solitons},$$
$$v \in (c_+; v_+), \qquad \text{'fast' solitons}.$$

The upper limit on the speed of propagation of the gap solitons being equal to δ rather than 0, if δ is negative, has a simple explanation. The phase mismatch was introduced through (2.27) by assuming that the evolution of the wave amplitude occurs on the slow $O(\epsilon)$ time scale. As the phase speed of the travelling wave v becomes close to δ the evolution on the slow time scale ceases to occur at the assumed order and the next order of slowness must be taken into account. In other words, the difference $|v-\delta|$ must be $O(1)$ to ensure validity of the asymptotic scheme employed.

4.1. *'Fast' waves*

The region of existence of the 'fast' solitary waves is limited from above by the value v_+ corresponding to a 'peaked soliton' with a singularity at the crest. To investigate its type we assume, as suggested by numerics, that the internal wave field $b(\xi)$ remains smooth. Differentiating the first equation (4.2) with respect to ξ results in

$$2\left(a_s - \frac{v}{2}\right) a_s' = b_s'. \tag{4.3}$$

At $v = v_+$ the multiplier in the parentheses equals zero at the crest, hence the height of the limiting wave is given by

$$b_+ = -\frac{v_+^2}{4}, \quad \Rightarrow \quad a_+ = \frac{v_+}{2}; \tag{4.4}$$

b_+ corresponds to the trough of the internal wave as $b_s' = 0$. Expanding (4.3) in Taylor series with respect to ξ, assuming that the reference point of the coordinate system is the crest/trough of the wave and taking into account (4.4), leads to

$$a_\pm' = -\sqrt{\frac{b_s''}{2}}\,\mathrm{sgn}(\xi) \qquad \text{as} \qquad \xi \to \pm 0, \tag{4.5}$$

where $a_\pm'$ is understood as the left-/right one-sided derivative. The limiting wave has a jump of the first derivative at the crest of the vorticity wave component, i.e. its profile exhibits a sharp corner. The internal wave component $b(\xi)$ remains smooth similar to the shallow-water case. Our asymptotic model ceases to be applicable near the singularity, nevertheless, the emergence of such a singularity in the asymptotic model suggests the formation of a nonlinear critical layer near the surface, as the horizontal speed of the fluid particles swept by the wave approaches its phase speed v.

Examples of the 'fast' solitary wave profiles, moving with different speeds in deep water, are shown in figure 3. The dependence of the solitary wave velocity v and its characteristic width λ on the amplitude of the a-component are plotted in figure 4 for several values of δ. Wave speed increases monotonically with the increase of $\max(a_s)$. The width λ, understood as the spatial span of the a-component at the level $\max(a_s)/2$, decreases monotonically with the growth of its amplitude or speed. The spatial structure of the soliton is further discussed below in § 4.5.

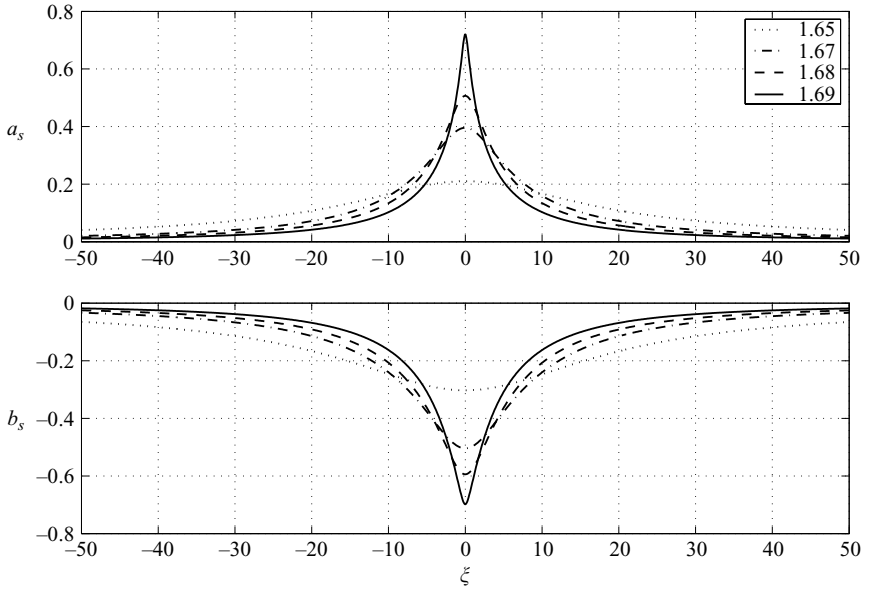

FIGURE 3. Profiles of the 'fast' solitary waves in deep water, $\delta = 1$. The values of corresponding soliton speeds v are shown in the box.

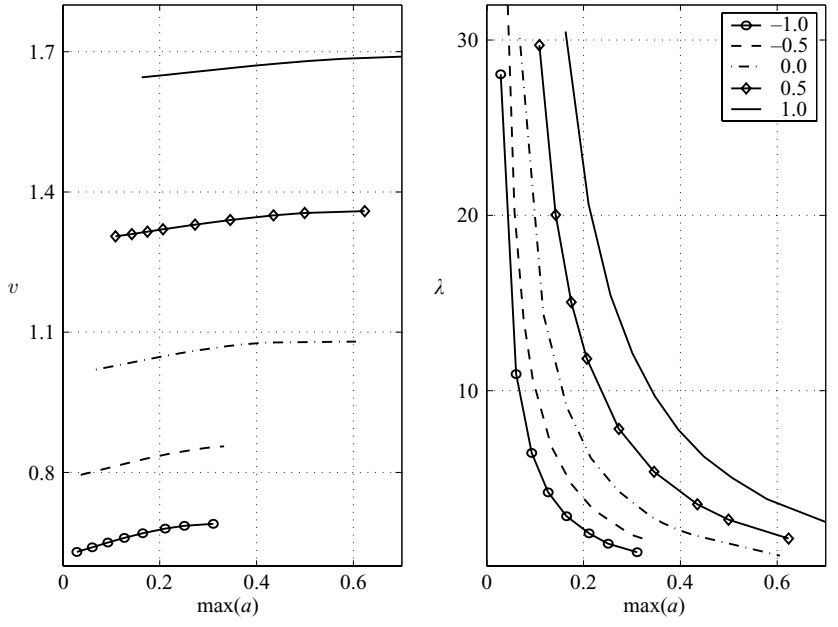

FIGURE 4. 'Fast' wave speed v and width λ vs. max(a_s) in deep water for different values of the phase mismatch δ (see the box).

4.2. *Gap solitons*

Examples of computed profiles of 'gap solitons' in deep water for $\delta = 1$ are shown in figure 5. They are more localized than the 'fast' ones, the core of the wave being better distinguished from the peripheral regions. The dependence of speed v and width λ on

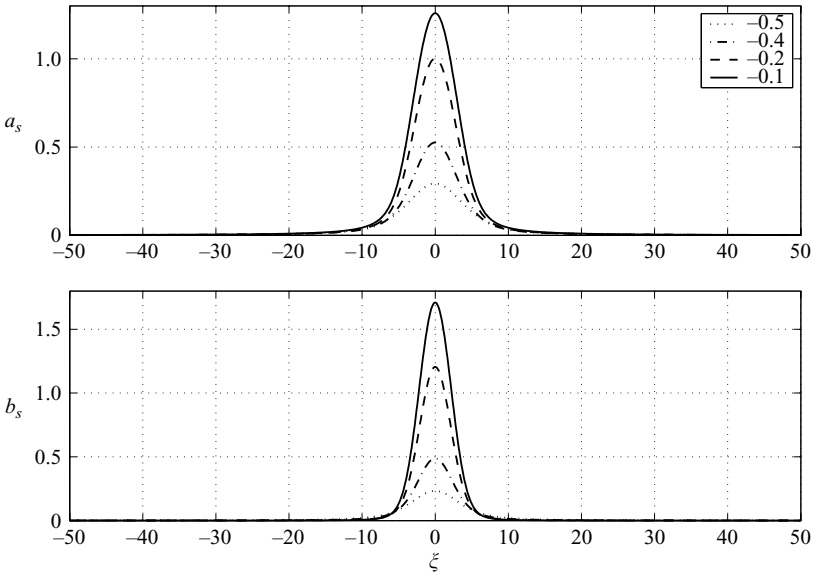

FIGURE 5. Profiles of the 'slow' solitary waves in deep water, $\delta = 1$. The values of corresponding soliton speeds v are shown in the box.

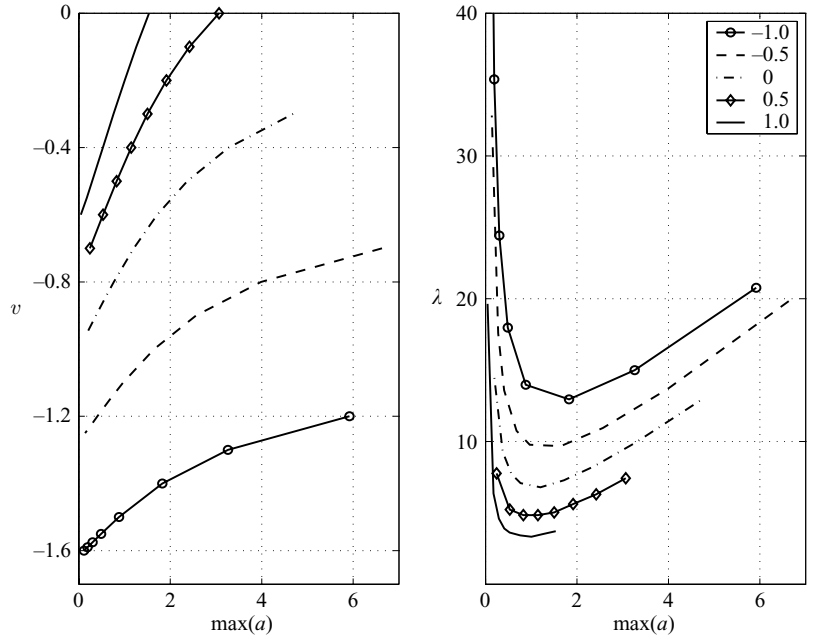

FIGURE 6. 'Slow' wave speed v and width λ vs. max(a_s) in deep water for different values of the phase mismatch δ (see the box).

the height of the a-component are plotted in figure 6 for several values of δ. Note that the dependence of the width λ on the wave height is not monotonic. This peculiar behaviour is observed for the 'gap solitons' in water of finite depth as well, although it becomes less pronounced as the depth decreases and disappears completely in the

shallow-water limit. The spatial structure of the solution is further discussed below in § 4.5.

4.3. *Decay at the periphery*

At the periphery of the solitary wave the amplitude decreases, (4.2) decouple and become close to the Benjamin–Ono(BO)/Joseph models, with typical $\sim\xi^{-2}$ or $\sim\exp(-|\xi|)$ decay as $|\xi|\to\infty$ (Benjamin 1967; Joseph 1977). From (4.2)

$$a_s = \frac{v}{2}\left(1 \pm \left(1 + \frac{4b_s}{v^2}\right)^{1/2}\right), \tag{4.6a}$$

$$(v - \delta + \tilde{\mathscr{L}})b_s + \frac{v}{2}\left(1 - \left(1 + \frac{4b_s}{v^2}\right)^{1/2}\right) = 0. \tag{4.6b}$$

The root with the negative sign must be taken in (4.6), otherwise the amplitudes a_s and b_s cannot vanish simultaneously, and the solution thus obtained does not describe a solitary wave.

At the periphery of the solitary wave the square roots in (4.6*a*), (4.6*b*) can be expanded in powers of $|b/v^2| \ll 1$ with just two terms providing sufficient accuracy:

$$a_s = -\frac{b_s}{v} + \frac{b_s^2}{v^3}, \tag{4.7a}$$

$$\left(v - \delta - \frac{1}{v} + \tilde{\mathscr{L}}\right) b_s + \frac{b_s^2}{v^3} = 0. \tag{4.7b}$$

After a scaling transformation (4.7*b*) becomes a stationary BO/Joseph equation specifying the amplitude of the solitary wave moving with the speed

$$\kappa = \frac{1}{v}(v - c_-)(v - c_+), \tag{4.7c}$$

where c_-, c_+ are the boundaries of the linear wave spectrum. Therefore, one could expect that the behaviour of the solitary wave solutions of (2.31) will be similar to that in the classical models, i.e. the waves will decay as $|\xi|\to\infty$ in a power-like manner in deep water and exponentially in the case of finite depth.

4.4. *'Delocalized solitons'*

Numerics also revealed the existence of soliton-like solutions to (4.2) for $\delta > 0$, within part of the interval $v \in (0,\ \delta)$. At first sight this result looks surprising, as there always exist linear harmonic waves propagating with the same speed. A solitary wave, thus, should be in resonance with a harmonic wave, which normally leads to the emission of the latter and the radiative damping of the former. Due to this mechanism, no steady solitary wave normally travels with speed equal to that of any harmonic wave. The profiles of the waves seem to be similar to those of the 'gap solitons', i.e. *a*- and *b*-components of the field have the same polarities in the core, the amplitude growing very fast with the speed increase. Yet, there are two striking differences, which become obvious when the area close to the ξ-axis is magnified. First, as the *a*-component of the wave field remains positive, the *b*-component changes its sign at a certain distance from the crest (see figure 7).

Second, at the periphery of the wave small oscillations are clearly visible (see figure 8). The amplitude of the tail oscillations is extremely small even in water of intermediate depth and they almost vanish as the depth of the fluid increases and the integral operator (2.29*b*) becomes close to (3.1). The oscillations still exist, but are

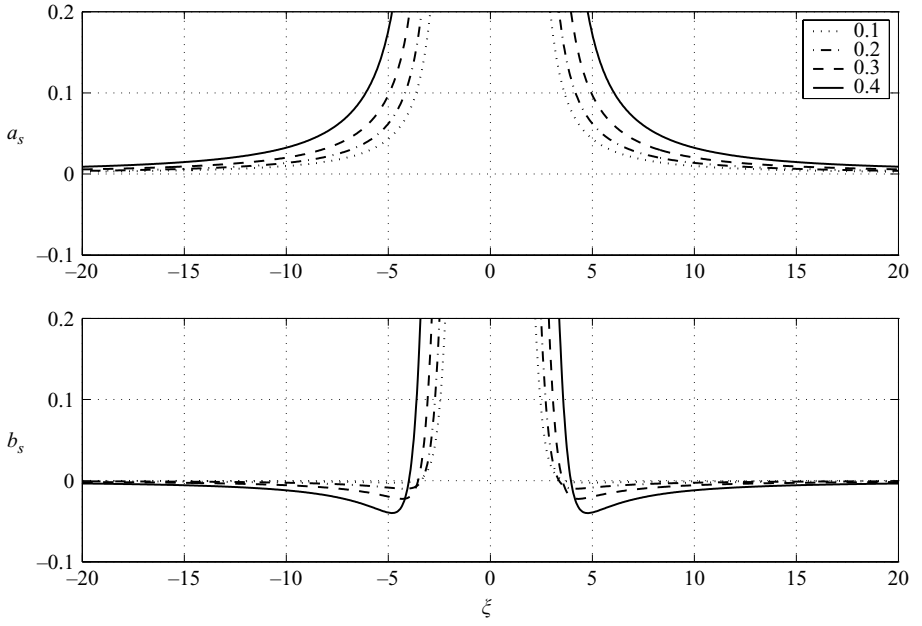

FIGURE 7. 'Delocalized' solitary wave profiles in deep water, magnified. $\delta = 1$, values of v corresponding to the different curves are given in the box.

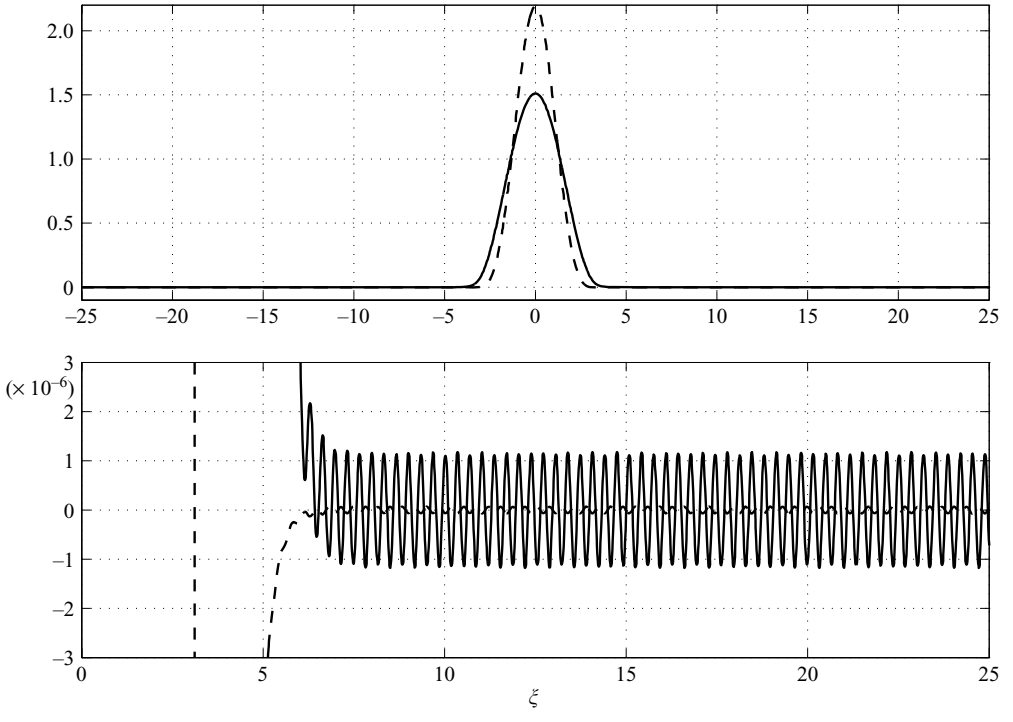

FIGURE 8. Delocalized solitary wave profile in finite-depth water, $D_* = 1$, $\delta = 2$, $v = 0.05$

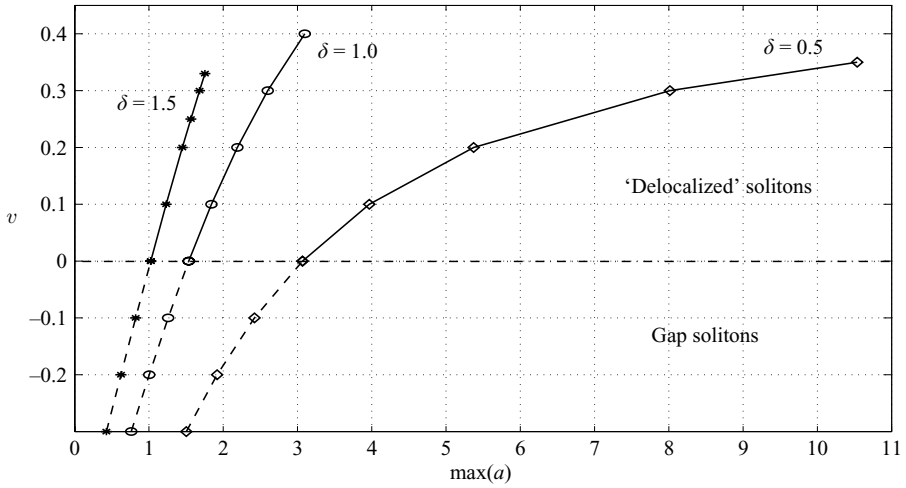

FIGURE 9. Velocity vs. amplitude for 'delocalized solitons' in deep water for different values of the phase mismatch.

not visible unless very special techniques are employed. The solitary waves resonant with the linear spectrum are, in fact, the so-called 'delocalized' solitons, similar to those studied by Grimshaw & Joshi (1995), Boyd (1991), Akylas & Yang (1995) and many others within the framework of higher-order (e.g. fifth-order KdV) evolution equations. A completely different approach was used by Iooss & Kirrman (1996), Iooss (1999), Iooss, Lombardi & Sun (2002) and others to study capillary–gravity waves of permanent form and steady waves at the interface of two fluids with different densities. By representing the Euler equations as a dynamical system and using the normal-form formalism (see e.g. Kirchgässner 1988), the authors proved rigorously the existence of steady solitary waves in these systems, including some examples with algebraic core and oscillatory tails (see Dias & Iooss 2003 for a review). All these studies were confined to potential fluid flows and strictly steady solitary-like patterns. The interest in such patterns was purely mathematical: it is, indeed, a mathematical challenge to find exponentially small tails typical of such patterns. However, nobody expects such symmetric double-tailed structures to survive in an evolutionary setting. We will come back to this point in the next subsection.

The origin of the 'delocalized solitons' and their affinity with the gap ones is most clearly revealed by figure 9: samples of nonlinear dispersion curves of the 'delocalized soliton' for several values of the mismatch δ shown as solid lines are the direct continuation of dispersion curves of the gap solitons of § 4.2 shown as dashed lines. The existence of 'delocalized solitons' proves to be strongly dependent on the kernel of the dispersion operator $\tilde{\mathscr{L}}$ in (4.2), and ultimately, on the water depth. Indeed, in the shallow-water limit ($\tilde{\mathscr{L}} = \tilde{\mathscr{L}}_{shallow} = \partial_{xx}$) they do not exist at all (see Voronovich *et al.* 1998*a*). In deep water, they seem to occupy the whole interval $(0, \delta)$ of the possible phase speeds, and the oscillatory tails are exponentially small. In water of finite depth $\tilde{\mathscr{L}}$ has the kernel given by (3.8*b*), which implies that $\tilde{\mathscr{L}} \to \tilde{\mathscr{L}}_{shallow} \equiv \partial_{xx}$ in the limit $D_* \to 0$. At the same time, in the limit $D_* \to \infty$ the kernel is asymptotically close to $|k|$ and, hence, $\tilde{\mathscr{L}}$ tends to the Hilbert transform. The intermediate nature of the Joseph operator manifests itself in the range of existence of the 'delocalized solitons': the span of their speeds contracts from $(0, \delta)$ to zero, as the water depth D decreases from infinity to zero.

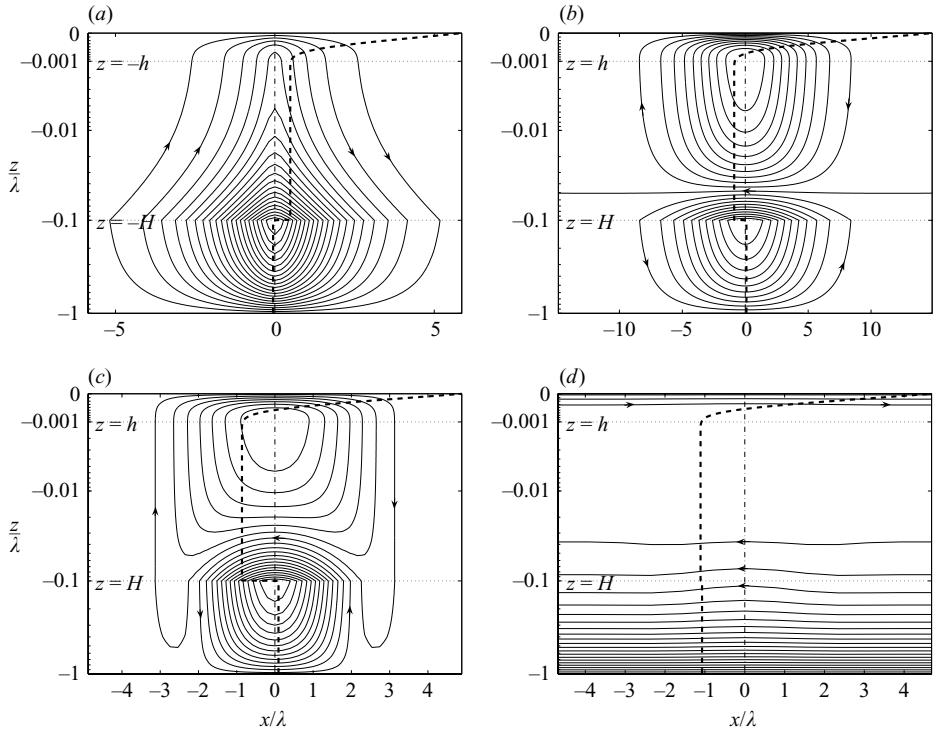

FIGURE 10. Spatial structure of the solutions. Streamlines of the perturbation field (a, b, c) and the total velocity field (d) $(D = 1,\ \delta = 2,\ \epsilon = 0.1)$: (a) 'fast' solitons $(v = 1.74)$; (b) 'slow' solitons $(v = -0.6)$. (c) 'delocalized' solitons $(v = 0.19)$. (d) Sketch of the total velocity field (current plus perturbation) for the 'delocalized' solitons $(v = 0.19)$ in the laboratory frame of reference. Bold dashed lines indicate the horizontal velocity profile of the perturbation (a, b, c) and the total field (d) in the soliton maximum.

4.5. *Spatial structure of the solutions*

In the previous subsections we investigated the classes of possible solutions within the framework of our asymptotic model and what these solutions look like in terms of non-dimensional amplitudes a and b. The issue of the spatial structure of the solutions found in the original physical variables and what this implies from the viewpoint of observations in different parts of the water column merits special consideration. Here, in addressing the issue, we confine ourselves to outlining just a few key points in a very brief discussion.

First, to interpret figures 3–9 already discussed, it is appropriate to recall that b is normalized amplitude of the internal gravity wave mode or deflection of the density interface taken with the negative sign, while a is normalized amplitude of the vorticity mode or normalized perturbation of the surface velocity.

The best way to give an idea of the spatial structure of different solutions would be to plot representative velocity fields. However, to represent graphically the velocity field distributions is a formidable challenge because, first, the spatial scales h, H, D and λ could be widely separated, and second, the perturbation velocity scaling varies very significantly: from $O(\epsilon)$ in the uppermost layer to $O(\epsilon^3)$ in the bottom layer. In figure 10 we attempt to overcome the difficulty by plotting the streamlines of representative samples of the three basic types of soliton solutions and employing

special non-uniform scaling. For the example we assume the surface current profile to be prescribed by the error function. For all solutions under consideration we choose the same set of parameters: $D = 1$, $\delta = 2$, $\epsilon = 0.1$. Since drawing the streamlines at the true scale is not illuminating because of the mentioned wide separation of scales, we compress the picture in the horizontal direction and employ the following non-uniform scaling along the vertical: we map $z \in [0, -\infty]$ onto uniformly varying $\eta \in [0, -\infty]$ by the formula

$$\eta = -\log(1 - z/h).$$

The scale is almost uniform in the uppermost layer and approximately logarithmic in the middle and bottom ones. To circumvent the problem caused by the presence of vastly different velocity magnitudes we adapt the step between the streamlines to show motions in the nearly stagnant part of the flow as well. Thus, the streamline density and direction do not allow one to quantify the true velocity; nevertheless these pictures overall give a good qualitative idea of the spatial structure of the motions. Most vividly this 'topological' structure could be seen in the perturbation-only field (i.e. with the mean flow comprising the surface current and the flow resulting from the motion of the coordinate frame, subtracted) in the frame of reference moving with the wave, as shown in figure 10(*a–c*). It easy to infer that the fast solitons have less pronounced surface manifestations compared to the slow and delocalized ones of comparable amplitude at the pycnocline. The perturbations of the surface velocity due to the fast solitons are in phase with the velocity at the density interface, in contrast to the slow and delocalized ones. To give a better idea of the horizontal velocity its vertical distribution in the soliton maximum is plotted by a bold dashed line. The horizontal scale is arbitrary, the reference is provided by the vertical dot-dashed line which indicates the zero of this velocity component. The horizontal velocity, as expected, has a break at the density jump. Figure 10(*b*, *c*) shows both the affinity of the slow and delocalized solitons and the subtle features by which they could be distinguished either in numerical simulations or experiments.

However, it is worth noting that in reality, i.e. in any experiment (including numerics), the raw picture of fluid motion will look dramatically different for a number of reasons. First, all closed streamlines disappear in the laboratory frame. The larger the wave celerity, the less pronounced the observed motion will look in the records and vice versa. Second, bringing back into the picture the much stronger mean current obviously makes the perturbation field less visible. Third, for the full velocity field the separation of scales in the velocity magnitudes increases even further. The full effect of the first two factors is shown in figure 10(*d*), where the delocalized soliton of figure 10(*c*) is presented in the laboratory frame of reference in the presence of the mean current. Although the effect of the third factor was mitigated by the non-uniform scaling adopted, the soliton becomes quite inconspicuous: there are only slightly disturbed horizontal lines. Note that in figure 10(*d*) the perturbation has been exaggerated; therefore, this figure should be viewed more as a sketch than a true plot of the solution. All this suggests that the solitary waves resulting from the direct resonance interaction are very difficult to discern in any sort of data without a special effort.

4.6. *Oscillatory tails*

Asymptotics of the wave field at large ξ can be found by a method similar to that used by Akylas & Yang (1995) to find asymptotic solutions of the forced KdV equation. The speed of 'delocalized' solitons lies within the linear spectrum; therefore, κ in (4.7*c*) is negative. Fourier transform of (4.7*b*) (for lucidity we confine our attention to

the deep-water limit) results in

$$\widetilde{b}_k = -\frac{1}{|k| - |\kappa|} \frac{\widetilde{(b_s^2)}_k}{v^3} = -\frac{1}{v^3} \frac{1}{|k| - |\kappa|} \int_{-\infty}^{\infty} \widetilde{b}_q \widetilde{b}_{k-q} \, \mathrm{d}q, \tag{4.8}$$

where $\widetilde{b}_k$ is the kth Fourier component of $b_s(\xi)$. The inverse Fourier transform of (4.8) yields an integral equation

$$b_s(\xi) = -\frac{1}{2\pi v^3} \int_{-\infty}^{\infty} \frac{\mathrm{e}^{\mathrm{i}k\xi}}{|k| - |\kappa|} \widetilde{(b_s^2)}_k \, \mathrm{d}k \tag{4.9}$$

from which, assuming that $\widetilde{(b_s^2)}_k$ is specified primarily by the soliton's core, asymptotic expressions for the solitary wave tails can be easily deduced. The singularity in the spectrum of the solution corresponds to the tail oscillations.

To find the tail asymptotics, we first split the integral into two: over positive and negative k. The second one can be further transformed:

$$-\frac{1}{2\pi v^3} \int_{-\infty}^{0} \frac{\mathrm{e}^{\mathrm{i}k\xi}}{-k - |\kappa|} \widetilde{(b_s^2)}_k \, \mathrm{d}k = -\frac{1}{2\pi v^3} \int_{0}^{\infty} \frac{\mathrm{e}^{-\mathrm{i}k\xi}}{k - |\kappa|} \widetilde{(b_s^2)}_k^* \, \mathrm{d}k. \tag{4.10}$$

The equality $(b_s^2)_k^* = (b_s^2)_{-k}$, valid since $b^2(\xi)$ is real, was used. Hence,

$$b_s(\xi) = -\frac{1}{2\pi v^3} \int_{0}^{\infty} \frac{\mathrm{e}^{\mathrm{i}k\xi}}{k - |\kappa|} \widetilde{(b_s^2)}_k \, \mathrm{d}k + \text{c.c}, \tag{4.11}$$

where c.c. stands for complex conjugate. On rearranging the terms in the integrand, (4.11) can be presented in the form

$$b_s(\xi) = -\frac{1}{2\pi v^3} \left(\widetilde{(b_s^2)}_{|\kappa|} J_1 - \widetilde{(b_s^2)}_{|\kappa|} J_2 + J_3 \right) + \text{c.c.}, \tag{4.12a}$$

where $J_{1..3}$ designate the integrals

$$J_1 = \int_{-\infty}^{\infty} \frac{\mathrm{e}^{\mathrm{i}k\xi}}{k - |\kappa|} \, \mathrm{d}k, \quad J_2 = \int_{-\infty}^{0} \frac{\mathrm{e}^{\mathrm{i}k\xi}}{k - |\kappa|} \, \mathrm{d}k, \quad J_3 = \int_{0}^{\infty} \frac{\mathrm{e}^{\mathrm{i}k\xi}}{k - |\kappa|} \left(\widetilde{(b_s^2)}_k - \widetilde{(b_s^2)}_{|\kappa|} \right) \mathrm{d}k. \tag{4.12b}$$

Note that now only the first integral, J_1, in (4.12b) contains the singularity, whereas the other two are regular and can be approximated at large values of ξ by the Laplace method. After performing the necessary calculations the result is

$$-\widetilde{(b_s^2)}_{|\kappa|} J_2 + J_3 + \text{c.c.} = 2 \frac{\widetilde{(b_s^2)}_0}{|\kappa|^2 \xi^2} + o\left(\frac{1}{\xi^2} \right). \tag{4.13}$$

Equation (4.13) describes the power-like tail decay typical of the Benjamin–Ono solitons.

The integral J_1 can be evaluated by employing Jordan's lemma on the complex k-plane. The path of integration must be chosen in accordance with the casuality principle, as is common in studies of the radiative damping of moving perturbations in fluids or electromagnetic waves in plasmas (Landau 1946). Let us first consider a free solitary wave moving in a medium otherwise at rest and being in resonance with a linear wave. The linear waves of (2.31) have negative dispersion, i.e. their phase speed decreases with the wavenumber. The group speed

$$c_g = \frac{\partial \omega}{\partial k} = \frac{\partial (vk)}{\partial k} = v + k \frac{\partial v}{\partial k}, \tag{4.14}$$

hence, is smaller than the speed of the radiating solitary wave, $c_g < v$. The emitted radiation is lagging behind the soliton, and there must be no radiation ahead of the wave, i.e. at $\xi \to +\infty$, by virtue of the causality principle. The path of integration in the complex domain must then consist of a straight line parallel to the real axis and crossing the imaginary one at $\varepsilon > 0$, so that

$$k = \mathrm{Re}[k] + \mathrm{i}\varepsilon \quad \text{and} \quad \exp\{\mathrm{i}k\xi\} = \exp\{\mathrm{i}\,\mathrm{Re}[k]\xi\}\exp\{-\varepsilon\xi\} \to 0, \quad \xi \to +\infty \tag{4.15}$$

where Re designates the real part, and a semicircle in the upper plane, if ξ is positive, and in the lower plane if it is not. The contour must be passed in the clockwise direction for negative ξ and counterclockwise for positive, the value of the integral determined by the residues in the singular points of the integrand. The value of J_1 is obtained by taking the limit $\epsilon \to 0$.

The only pole of the integrand in J_1 is situated on the real axis at $k = |\kappa|$; therefore

$$\int_{-\infty}^{\infty} \frac{\exp\{\mathrm{i}k\xi\}}{k - |\kappa|}\,\mathrm{d}k = \begin{cases} 0, & \xi > 0 \\ -2\pi\mathrm{i}\exp\{\mathrm{i}|\kappa|\xi\}, & \xi < 0. \end{cases} \tag{4.16}$$

Finally, the expression for the tails of the delocalized solitons in deep water can be written as (by virtue of (3.9) $|\kappa| = 2/v \gg 1$)

$$b_s(\xi) = \begin{cases} -\dfrac{\widetilde{(b_s^2)}_0}{\pi v^3 |\kappa|^2 \xi^2} + o\left(\dfrac{1}{\xi^2}\right), & \xi > 0 \\ \dfrac{2}{v^3}\,\mathrm{Re}\left[\mathrm{i}\exp\{\mathrm{i}|\kappa|\xi\}\,\widetilde{(b_s^2)}_{|\kappa|}\right] - \dfrac{\widetilde{(b_s^2)}_0}{\pi v^3 |\kappa|^2 \xi^2} + o\left(\dfrac{1}{\xi^2}\right), & \xi < 0. \end{cases} \tag{4.17}$$

We stress that (4.17) describes an asymmetric profile. The solitary wave has an oscillatory tail only behind it, while ahead the medium remains unperturbed. This result at first sight contradicts our numerical computations, where all solitary wave profiles were found to be symmetric with respect to the crest. To explain this contradiction let us recall that in the course of numerical computations we were looking for stationary solutions of (4.6*b*), whereas (4.17) describes a radiating, non-stationary soliton. 'Delocalized' solitons found numerically represent, in fact, just one period of the periodic cnoidal-like wave in the strongly nonlinear limit, which can be viewed as a sequence of solitary waves separated by a very large distance. Hence, the stationary solitary waves obtained in the numerical experiments are indeed emitting backward, but at the same time they absorb the radiation emitted by the preceding solitary wave. The energy losses due to Landau damping are then balanced by the absorption and the wave is stationary.

Equation (4.17) indicates that the amplitude of the oscillations in the tail of the soliton is proportional to the amplitude of the resonant Fourier harmonic $\left(b_s^2\right)_{|\kappa|}$. In finite-depth water solitary waves are much more localized, their tails decaying exponentially fast. This results in a much wider spectrum and more easily detectable tail oscillations. The span of speeds of the 'delocalized' waves is closely connected with their localization in the Fourier and ξ-space, which explains why the former contracts as the depth decreases.

Thus, we have found long-lived quasi-stationary radiating solitary waves, which, as we show below, will feature prominently in evolution scenarios.

5. Evolution of localized pulses

Solitary waves represent, probably, the most interesting class of solutions of nonlinear evolution equations. They are long-lived and attractive, i.e. an arbitrary localized pulse tends to evolve into a set of solitary waves plus, possibly, a wavetrain of harmonic oscillations. The latter is subject to dispersion; its amplitude decreases with time. In the solitary wave, on the contrary, the effect of dispersion is counterbalanced by the nonlinearity, which results in the much longer lifespan. In a sense solitary waves represent long-time asymptotics for a wide class of solutions of the initial value problem at large times. Whatever the initial conditions, after a sufficiently long time harmonic waves become almost unnoticeable in the wave field, while the solitary ones persist. This argument is corroborated well by numerous field observations in the ocean. Long internal waves, for example, are quite often observed in the ocean as solitary-like waves, rather than periodic wave modes, the standard models being KdV/Benjamin–Ono/Joseph equations (see e.g. Ostrovsky & Stepanyants 1989). To check whether the solitary wave solutions of (2.31) indeed represent the asymptotics of the evolution of initial localized pulses, and, in particular, to clarify the role of radiating solitary waves, we carried out extensive numerical simulations. Equations (2.31) were integrated in time starting with the pulses having the shape of the solitary wave computed in § 4, with the width increased by a factor 4 and the amplitude by factors ranging from 0.4 to 2.5. The resulting localized pulses do not represent a solution to (2.31) and have to evolve in the course of propagation. The numerical scheme employed is based on the pseudospectral method with respect to the spatial variable and on the Runge–Kutta scheme with respect to time. Employing the Fourier transform we rewrite (2.31) in the spectral form

$$\dot{\widetilde{a}}_k = \mathrm{i}k[-(\widetilde{a^2})_k + \widetilde{b}_k], \tag{5.1a}$$

$$\dot{\widetilde{b}}_k = \mathrm{i}k[\widetilde{a}_k + (-\delta + \mathscr{L}_k)\widetilde{b}_k], \tag{5.1b}$$

where the dot denotes the derivative with respect to time. Equations (5.1) represent a system of nonlinear ordinary differential equations, which were solved numerically by the Runge–Kutta method, the computation of the nonlinear term being performed at each step using the FFT (fast Fourier transform) algorithm. To remove the aliasing errors which occur due to this nonlinear operation the upper half of the Fourier spectrum was zeroed after each step (Canuto filtering, see e.g. Canuto *et al.* 1988).

The simulations show that the outcome of the evolution of the localized pulse strongly depends on the pulse's initial amplitude and width. The pulses having the initial amplitudes below a certain threshold, which we refer to as 'subcritical', evolve into a set of solitary waves and a small wavy tail, whereas the 'supercritical' ones develop a singularity at the forefront, which suggests wave breaking, although, of course, the asympotic model is no longer valid near the singularity. An example of subcritical evolution in deep water is shown in figure 11, the amplitude factor of the initial pulse being equal to 2.0. There are four solitary waves emerging from the initial pulse, two moving right and two left. The wave situated at $x = 90$ at $t = 50$ has field components of opposite signs, which distinguishes it as the 'fast' solitary wave. Two waves moving left have negative velocities and obviously are the gap solitons. Yet the highest wave at $x = 20$ at $t = 100$ also has positive velocity, but its field components have the same polarity. It is a clear manifestation of a 'delocalized' soliton in the evolutionary problem.

A similar outcome is typical of water of finite depth as well: again initial pulses evolve into a sequence of solitons, including 'delocalized' ones, provided their initial

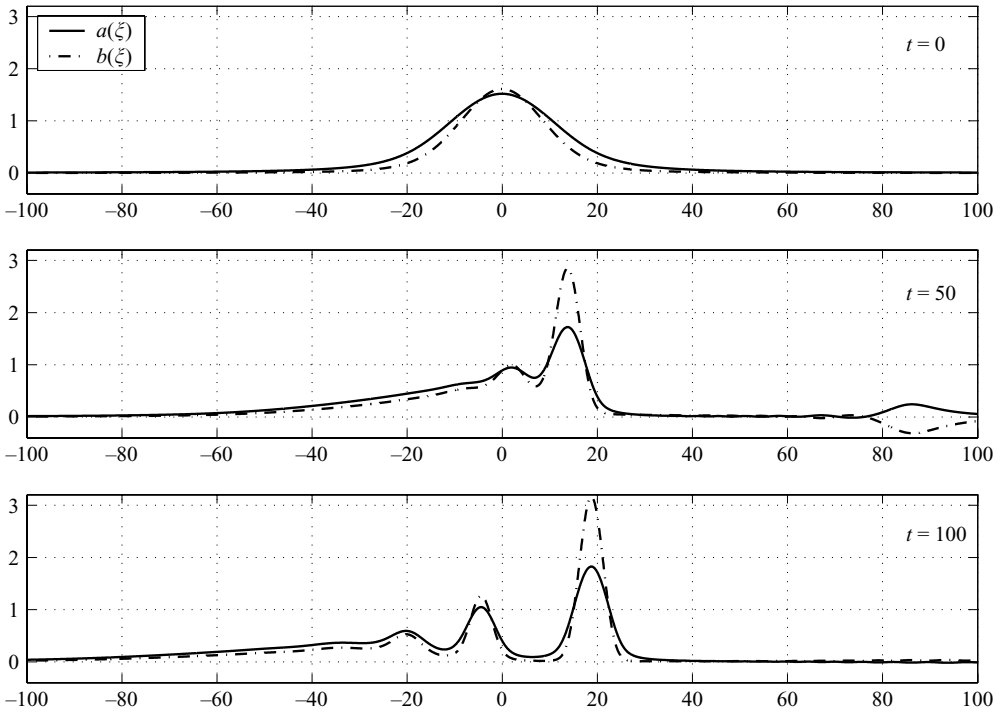

FIGURE 11. Evolution of a subcritical initial pulse in deep water, $\delta = 1$.

amplitude is below the threshold, and break otherwise. An example of the subcritical evolution in water of finite depth is shown in figure 12, with the 'delocalized' wave emerging with by far the largest amplitudes and moving to the right. The computations prove that 'delocalized' solitons do emerge in simulations as intermediate asymptotics of the initial value problem, and, moreover, typically they have the largest amplitude and, therefore, represent a physically very important class of solutions of (2.31). Of course, the number and the type of solitary waves emerging from the original pulse strongly depend on the initial values of the integrals (3.3). The radiating 'delocalized' solitons which tend to have larger amplitudes and, hence, correspond to larger values of the integrals of motion, emerge only if the initial values of the latter are above a certain threshold. In our calculations none emerged unless the amplitude of the initial pulse, i.e. a solitary wave stretched by the factor 4, was larger than 1.6 times the amplitude of the original solitary wave.

A typical example of the 'supercritical' evolution is shown in figure 13, the amplitude factor being 2.3 in this case. Similarly to the subcritical evolution, first a 'fast' solitary wave starts to emerge from the initial pulse, but instead of simply running away develops a singularity at the crest, the front becoming vertical at $t = 12$. Of course, the calculations have to be stopped at this stage as the amplitudes of the higher Fourier harmonics grow very fast, rendering the pseudospectral scheme employed inapplicable. The most probable reason for the instability seems to be the following: the amplitude of the 'fast' wave, which is expected to form, exceeds the amplitude of the 'peaked' soliton corresponding to the chosen values of the depth and the phase mismatch δ. Any attempt to form such a 'supercritical' wave would immediately result in instability. It is worth noting that the singularity develops only in the a-component of the wave field, while $b(\xi)$ remains smooth. Hence, the breaking would be observed

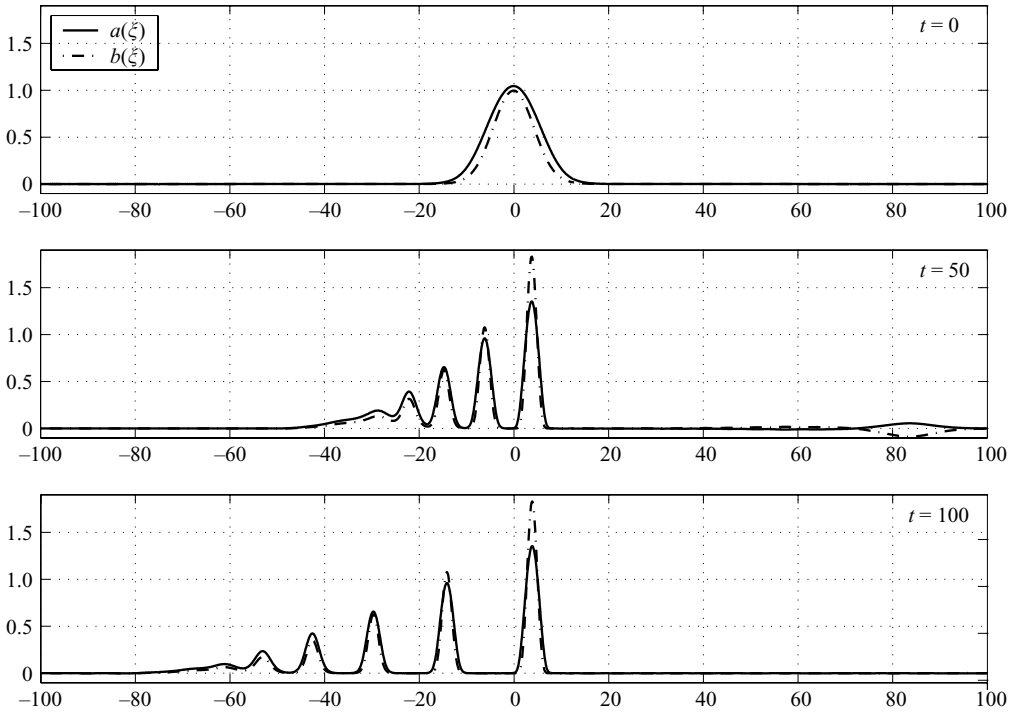

FIGURE 12. Evolution of a subcritical initial pulse in finite-depth water, $\delta = 2$, $D_* = 1$.

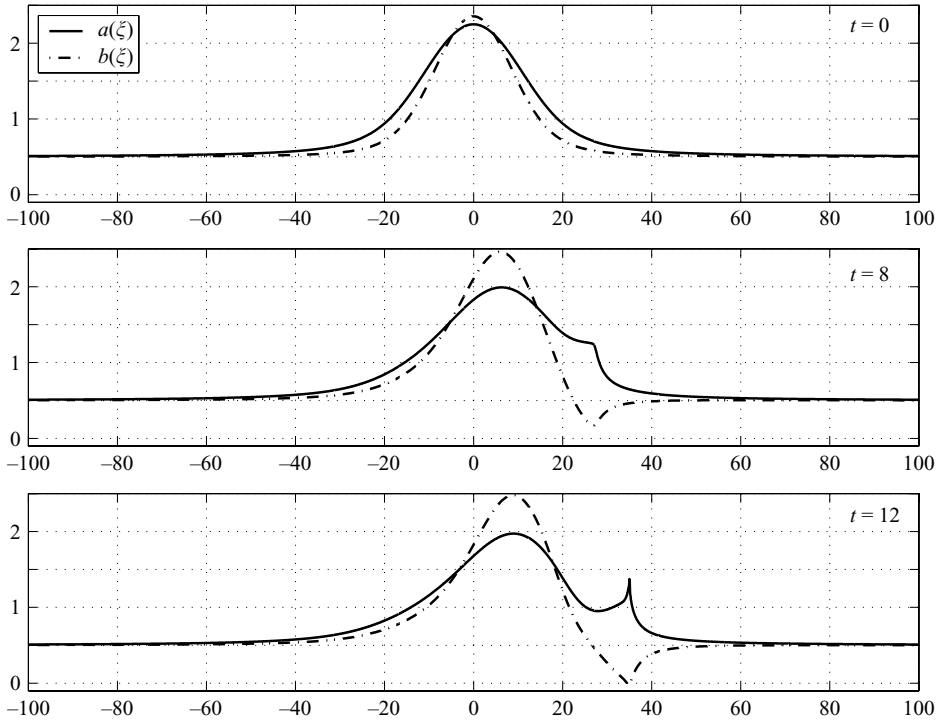

FIGURE 13. Evolution of a supercritical initial pulse in deep water, $\delta = 1$.

in the upper layer only, the motion at depth remaining regular. The possible outcome of the instability is difficult to tell, having been confined by the assumptions leading to (2.31). The solitary waves might still emerge after the breaking process is finished and a part of the initial pulse's 'mass' is lost to the vortices and turbulence. However, this question was not addressed and is beyond the scope of the present paper.

6. Discussion

Here we briefly summarise the results and discuss their context and possible implications. First, the study shows that the internal wave–shear flow resonance is a generic phenomenon which can occur in water of arbitrary depth and that the presence of quite a shallow surface current can change qualitatively the nonlinear dynamics of internal gravity waves even if the pycnocline depth far exceeds the penetration scale of the current. Although the resonance condition (2.27) is somewhat restrictive, especially when the balance (2.7) is taken into account, we expect the resonance to occur in natural basins, provided the stratification is comparatively weak or the current has considerable shear. Under the resonant conditions the interaction of internal waves with the current, rather than their own nonlinearity, is the key factor influencing the waves' dynamics. Even comparatively weak internal waves, which in the absence of the current would remain linear, can induce strong nonlinear effects, including 'peaked solitons' and breaking events just beneath the sea surface. Therefore, surface currents not only represent one of the principal factors in the amplification of internal waves surface signatures, but also could quite significantly affect the internal wave's own dynamics and, therefore, must be always recorded during the internal wave field observations and taken into account in the experimental data interpretations. The interpretation of the observations is not easy and straightforward. As exemplified by figure 10(*d*), the manifestations of radiating solitary waves in the laboratory frame of reference with the mean current being part of the picture are quite inconspicuous. In the real ocean the presence of the ambient-noise wave field makes discerning such solitary waves by chance practically impossible. Because of the large separation of scales involved, it is extremely difficult to find these motions, even by direct numerical simulations of full hydrodynamic equations, without precise prior knowledge of what to look at and what to expect.

In typical *in situ* observations the most commonly recorded characteristic is the pycnocline deflection. If a solitary-wave-type pattern on the interface is recorded and identified as such (in our context the most difficult bit), then it is easy to trace its origin even in the absence of any other measurements: the 'resonant' solitons are much shorter than the classical KDV/Benjamin–Ono/Joseph solitons of the same amplitude. If the variations of the surface velocity are also monitored, then it becomes possible to distinguish between fast and gap/delocalized 'solitons': the perturbations of the surface velocity are in phase with the pycnocline deflection for the former and in counterphase for the latter. Use of acoustics should enable one to make a finer distinction between slow and delocalized radiating solitary waves by combining ADCP measurements with spatial structure analysis of the type presented in § 4.5.

It is appropriate to recall the basic physics of the resonance in deep/finite-depth water, which is similar to that in shallow seas. Internal waves originating from the density interface produce a pressure perturbation in the upper layer moving with the flow. The induced pressure wave causes a velocity perturbation, which is accounted for in the model as a vorticity wave mode. Of course, the feedback influence, which makes the dynamics of the internal wave nonlinear, is present as well. This basic mechanism works similarly both in shallow and deep/finite-depth water and the

resulting wave patterns are quite similar, apart from the one, but striking, difference we discuss below.

Although Voronovich *et al.* (1998*a*) have shown explicitly that no stationary waves can exist outside the gaps in the spectrum of linear waves in shallow water, in water of finite depth we found 'delocalized solitons' travelling with speeds belonging to the range of linear waves. In itself, the fact of their existence is not particularly surprising: similar stationary solutions are common in many systems where several wave modes interact (e.g. Boyd 1991). The focus of our study is the role they play in the evolution. Such solitary waves are expected to radiate linear harmonics and decay due to the Landau damping mechanism and this, indeed, happens. Yet, the rate of energy loss being asymptotically small, the radiating solitary waves prove to be quasi-stationary, i.e. long-lived patterns. Thus, these are effectively not so different from the classical ones and do represent intermediate asymptotics in the temporal evolution of the localized pulses. Moreover, for a wide class of initial perturbations, they emerge as by far the highest solitary waves. Therefore, not only should such objects be accounted for in all studies of wave evolution, but for some aspects of the evolution they often represent the dominant feature. The issue, certainly, needs further study. However, we believe, that the phenomenon is generic and we expect that in all systems admitting 'delocalized solitons' with asymptotically small tails, they represent intermediate asymptotics in the temporal evolution, but are unaware of any studies concerned with this issue and, therefore, at present cannot provide any evidence to support our conjecture.

The role played by the quasi-stationary radiating solitary waves in nonlinear field evolution is in many respects similar to that played by the quasi-modes in linear dynamic in shear flows (Shrira & Sazonov 2001). Normally, in a linear setting the large-time asymptotics of arbitrary initial conditions are represented by a sequence of wave packets corresponding to discrete eigenvalues of the system, while in nonlinear systems, admitting soliton solutions, these correspond to the discrete spectrum and represent similarly dominant large-time asymptotics (for an integrable system this statement should be understood literally and not as a metaphor). In a linear setting the quasi-modes represent 'fictitious', weakly decaying due to Landau damping, discrete modes made up of a combination of continuous spectrum modes, which are shown to be intermediate (and often absolute) asymptotics of generic initial-value problems (Sazonov & Shrira 2003). However, there is an important distinction: the quasi-modes eventually tend to decay into a continuous spectrum, while the radiating solitary waves, as suggested by figure 9, will eventually turn into the usual 'gap solitons', that is into part of the discrete spectrum. It should be noted we have not simulated such a transformation of radiating solitons, since it represents a technical challenge and the asymptotic validity of our model breaks down for very small v. Perhaps this new phenomenon would be easier to examine first within the framework of a simpler model, say, fifth-order KdV.

In the context of internal waves, we, for the sake of simplicity, made a number of assumptions and now it is appropriate to discuss, how critical they are. The two-layer model of stratification was chosen as the simplest model exhibiting the desired phenomenon. The generalization of the results for an arbitrary continuous stratification is straightforward, provided the scaling assumptions hold. Although we ignored spanwise variability, three-dimensional effects are easily taken into account, provided their scale considerably exceeds the wavelengths. This would result in the KP-like modification of the second equation in (2.31), as in Voronovich *et al.* (1998*a*). However, the character of the evolution in such a KP-type extension of the model

has not been studied; we cannot exclude that in a certain range of parameters the planar solitary waves found might be transversally unstable. Horizontal homogeneity was assumed, although in reality large-scale variations of the thermocline strength and depth, bottom topography and current speed are quite common. If this is the case, the phase mismatch δ in (2.31) will depend on the streamwise coordinate and the evolution is not expected to differ qualitatively from the two basic scenarios described in Shrira *et al.* (2000). Either the waves would tend to disentangle from the current, decrease in amplitude and evolve into the true low-amplitude BO/Joseph solitons, or their steepness would grow resulting in the emergence of the 'peaked solitons' and breaking. A new interesting possibility is transformation of 'gap solitons' into the radiating ones and vice versa caused by inhomogeneity, as well as the evolution of steepening radiating solitary waves towards a parameter domain characterized by increasing radiation. However, the effects due to horizontal non-uniformities and their influence on the resonant wave dynamics are beyond the scope of the present paper and require a separate study.

The authors are grateful to D. Pelinovsky for helpful discussions. V. V. V. gratefully acknowledges partial financial support from the UCC Boole Centre for Research in Informatics. The work was also supported by INTAS 01-234.

Appendix A. Matching condition at the density jump interface

We begin with the standard system of equations for fluid motion in the form

$$\rho \mathscr{D} u + p_x = 0 \quad \left(\mathscr{D} = \frac{\partial}{\partial t} + u \frac{\partial}{\partial x} + w \frac{\partial}{\partial z} \right), \tag{A 1a}$$

$$\rho \mathscr{D} w + g\rho + p_z = 0, \tag{A 1b}$$

$$\mathscr{D} \rho = 0, \tag{A 1c}$$

$$u_x + w_z = 0, \tag{A 1d}$$

where $\boldsymbol{u} = \{u, w\}$, p are the total velocity and pressure, g is acceleration due to gravity and $\mathscr{D}$ is the material derivative. The equilibrium density of the fluid ρ_e is constant in the layers and has a finite jump at the moving interface $z = -H + \zeta\,(t, x)$.

First note that at the interface the tangential component of the pressure gradient must be continuous, i.e.

$$[p_x + \zeta_x p_z] = 0, \tag{A 2}$$

where as before

$$[f] = f^+ - f^-, \quad f^\pm = f(-H + \zeta \pm, 0) \tag{A 3}$$

denotes the jump of the variable f at the interface and $f^\pm$ are the values of the function f just above and below it. By definition the interface displacement $\zeta\,(t, x)$ is continuous at the interface. Then, multiplying (A 1*b*) by ζ_x, summing the result with (A 1*a*) and utilizing (A 2), we obtain

$$[\rho \Psi] + g[\rho]\zeta_x = 0, \quad \text{where} \quad \Psi = \mathscr{D} u + \zeta_x \mathscr{D} w. \tag{A 4}$$

Employing the definition (A 3) simple manipulations yield

$$\begin{aligned} [\rho\Psi] = \rho^+\Psi^+ - \rho^-\Psi^- &= (\rho^- + [\rho])(\Psi^- + [\Psi]) - \rho^-\Psi^- \\ &= \rho^-[\Psi] + \Psi^-[\rho] + [\Psi][\rho] \\ &= \rho^-[\Psi] + \Psi^+[\rho]. \end{aligned} \tag{A 5}$$

Therefore, (A 4) can be written as

$$[\Psi] + g\frac{[\rho]}{\rho_-}\zeta_x = -\Psi^+\frac{[\rho]}{\rho^-} \tag{A 6a}$$

or, by virtue of the definition of Ψ in (A 4),

$$[\mathscr{D}u] + [\mathscr{D}w]\zeta_x + g\frac{[\rho]}{\rho_-}\zeta_x = (\mathscr{D}u^+ + \zeta_x\mathscr{D}w^+)\frac{[\rho]}{\rho_-}. \tag{A 6b}$$

Under the Boussinesq approximation the right-hand side vanishes. Recall that

$$[\rho] = -\Delta\rho, \quad \rho^- = \rho_2,$$

then (A 6*b*) transforms into the required dynamic boundary condition condition (2.5*b*)

$$[\mathscr{D}u] + [\mathscr{D}w]\zeta_x - g'\zeta_x = 0 \quad \text{at} \quad z = -H + \zeta.$$

Here $g' = g\Delta\rho/\rho_2$ is reduced gravity.

Appendix B. Newton's iterations

To find localized solutions of (4.2) a numerical scheme based on the standard Newton method was employed. Excluding b_s from (4.2*b*) first we arrive at

$$\tilde{\Lambda}[a_s] = \tilde{\mathscr{N}}\left[a_s^2\right], \tag{B 1a}$$

where $\tilde{\Lambda}$ and $\tilde{\mathscr{N}}$ are linear operators:

$$\tilde{\Lambda}[a_s] = (v(v-\delta+\tilde{\mathscr{L}}) - 1)a_s, \quad \tilde{N}\left[a_s^2\right] = (v-\delta+\tilde{\mathscr{L}})a_s^2. \tag{B 1b}$$

Performing the Fourier transform of (B 1*a*) results in

$$\widetilde{a}_k = \frac{N_k}{\Lambda_k}\widetilde{\left(a_s^2\right)}_k, \tag{B 2a}$$

where

$$\Lambda_k = v(v-\delta) - 1 + vQ(k), \quad N_k = v - \delta + Q(k) \tag{B 2b}$$

are the Fourier images of the kernels of the original operators (B 1*b*).

At each step the next approximate value of the function a_s^{j+1} was assumed to be the sum of the previous approximation a_s^j and an unknown discrepancy η^j:

$$a_s^{j+1} = a_s^j + \eta^j. \tag{B 3}$$

The discrepancy was assumed to be sufficiently small compared to the approximation of the solution that (B 1*a*) might be linearized with respect to η. Thus, at the jth step of the iteration process we consider a linear equation

$$\tilde{\Lambda}\left[a_s^j\right] + \tilde{\Lambda}[\eta^j] = \tilde{\mathscr{N}}\left[\left(a_s^2\right)^j + 2a^j\eta^j\right], \tag{B 4}$$

with the terms quadratic in η^j neglected. Performing a Fourier transform of (B 4) results in

$$(\Lambda_k - 2N_k\tilde{\mathscr{A}}^j)\widetilde{\eta}_k^j = N_k\widetilde{\left(a_s^2\right)}_k^j - \Lambda_k\widetilde{a}_k^j. \tag{B 5}$$

Here $\tilde{\mathscr{A}}^j$ is the operator of convolution in k-space, which appears due to the term with the product of two functions occurring in x-space:

$$\tilde{\mathscr{A}}^j\left[\widetilde{\eta}_k^j\right] = \widetilde{a}_k^j * \widetilde{\eta}_k^j. \tag{B 6}$$

Solving (B 5), i.e. finding η^j, yields the next approximation to the solution a^{j+1} via (B 3).

To perform numerical computations one has to discretize the equations, i.e. substitute continuous functions a_s, η with the vectors of finite length composed of the values of the former at the points of a chosen grid, in both ξ- and k-spaces. In the discrete form the action of linear operators on a function generally corresponds to the multiplication of the vector by the matrix. The matrices corresponding to the operators $\tilde{\Lambda}$ and $\tilde{\mathcal{N}}$ have elements differing from zero only on the main diagonal, these being the elements of the vector obtained from the Fourier images of the corresponding operator kernels $\boldsymbol{L}_k$, $\boldsymbol{N}_k$. We use bold type to denote vectors and matrices. It is much less obvious how matrix $\boldsymbol{A}^j$ corresponding to the operator $\tilde{\mathscr{A}}^j$ looks like. To find $\boldsymbol{A}^j$ note that the element-by-element multiplication of two vectors which results in the vector with the components equal to the products of the corresponding elements of the multipliers (the subscript denotes the nth component of the vector)

$$(\boldsymbol{a} \odot \boldsymbol{\eta})_n = a_n \eta_n,$$

can be written as the product of a diagonal matrix $\mathrm{diag}(\boldsymbol{a}^j)$ by a column-vector $\boldsymbol{\eta}^j$

$$\boldsymbol{a}^j \odot \boldsymbol{\eta}^j = \mathrm{diag}(\boldsymbol{a}^j)\boldsymbol{\eta}^j$$

where the diagonal matrix $\mathrm{diag}(\boldsymbol{a}^j)$ is formed from the appropriately placed elements of the vector $\boldsymbol{a}^j$. Let $\boldsymbol{F}$ and $\boldsymbol{F}^{-1}$ be the matrices of the direct and inverse discrete Fourier transform, then the action of operator $\tilde{\mathscr{A}}^j$ can be accounted for as the successive product of the matrices by the discrepancy vector

$$\tilde{\mathscr{A}}^j\left[\tilde{\eta}_k^j\right] \longrightarrow \mathscr{F}[\mathrm{diag}(\boldsymbol{a}^j)\boldsymbol{\eta}^j], \tag{B 7a}$$

hence

$$\boldsymbol{A}^j\tilde{\boldsymbol{\eta}}_k^j \longrightarrow \boldsymbol{F}\,\mathrm{diag}(\boldsymbol{a}^j)\boldsymbol{F}^{-1}\tilde{\boldsymbol{\eta}}_k^j \Rightarrow \boldsymbol{A}^j = \boldsymbol{F}\,\mathrm{diag}(\boldsymbol{a}^j)\boldsymbol{F}^{-1}. \tag{B 7b}$$

On finding matrix $\boldsymbol{A}^j$, representing the operator of the convolution, we rewrite (B 5) in the form of a system of n inhomogeneous linear equations for the unknown components of the discrepancy vector $\tilde{\boldsymbol{\eta}}_k^j$:

$$\boldsymbol{M}^j\tilde{\boldsymbol{\eta}}_k^j = \boldsymbol{b}^j, \tag{B 8a}$$

where matrix $\boldsymbol{M}^j$ is given by the expression

$$\boldsymbol{M}^j = \mathrm{diag}(\boldsymbol{L}_k) - 2\,\mathrm{diag}(\boldsymbol{N}_k)\boldsymbol{F}\,\mathrm{diag}(\boldsymbol{a}^j)\boldsymbol{F}^{-1}, \tag{B 8b}$$

while the column vector on the right-hand side is

$$\boldsymbol{b}^j = \boldsymbol{N}_k\boldsymbol{F}\,\boldsymbol{a}^j \odot \boldsymbol{a}^j - \boldsymbol{L}_k\boldsymbol{a}_k^j. \tag{B 8c}$$

Here the symbol $\odot$ is used to denote the operation described above of the element-by-element multiplication of two vectors. We compute the convolution of two functions by multiplying their Fourier images and performing the inverse Fourier transform. The linear system (B 8) can then be solved by any standard method of numerical analysis.

REFERENCES

Akylas, T. R. & Yang, T.-S. 1995 On short-scale oscillatory tales of long-wave disturbances. *Stud. Appl. Maths* **94**, 1–20.

Benjamin, T. B. 1967 Internal waves of permanent form in fluids of great depth. *J. Fluid Mech.* **29**, 559–592.

Boyd, J. P. 1991 Weakly non-local solitons for capillary-gravity waves: Fifth-degree Korteweg-de Vries equation. *Physica* D **48**, 129–146.

Canuto, C., Hussaini, M., Quarteroni, A. & Zang, T. 1988 *Spectral Methods in Fluid Dynamics.* Springer.

Dias, F. & Iooss, G. 2003 Water-waves as a spatial dynamical system. *Handbook of Mathematical Fluid Dynamics*, pp. 443–499 (ed. S. Friedlander & D. Serre). Elsevier.

Grimshaw, R. H. J. & Joshi, N. 1995 Weakly nonlocal solitary waves in a singly perturbed Korteweg-de Vries equation. *SIAM J. Appl. Maths* **55**, 124–135.

Iooss, G. 1999 Gravity and capillary-gravity periodic travelling waves for two superimposed fluid layers, one being of infinite depth. *J. Math. Fluid Mech.* **1**, 24–61.

Iooss, G. & Kirrman, P. 1996 Capillary gravity waves on the free surface of an inviscid fluid of infinite depth. Existence of solitary waves. *Arch. Rat. Mech. Anal.* **136**, 1–19.

Iooss, G., Lombardi, E. & Sun, Sh. M. 2002 Gravity travelling waves for two superimposed layers, one being of infinite depth: a new type of bifurcation. *Phil. Trans. R. Soc. Lond.* A **360**, 2245–2336.

IOS/WHOI/ONR Internal Solitary Wave Workshop Papers 1999, 6th Edn, Papers Processed as of 12 May 1999. *WHOI Tech. Rep.* WHOI-99-07. http://www.whoi.edu/science/AOPE/people/tduda/isww/text/.

Joseph, R. J. 1977 Solitary waves in a finite depth fluid. *J. Phys.* A: *Math. Gen.* **10**, 1225–1227.

Kirchgässner, K. 1988 Nonlinearly resonant surface waves and homoclinic bifurcation. *Adv. Appl. Mech.* **26**, 135–181.

Klemas, V., Zheng, Q. & Yan, X.-H. 1998 *Internal Wave Online Atlas.* University of Delaware, http://atlas.cms.udel.edu.

Landau, L. 1946 On the vibrations of the electronic plasma. *Zh. Eks. Teoret. Fiz.* **16**, 574–586.

Leblond, P. H. & Mysak, L. A. 1979 *Waves in the Ocean.* Elsevier.

Nayfeh, A. H. 1993 *Introduction to Perturbation Techniques.* Wiley–Interscience.

Ostrovsky, L. A. & Stepanyants, Yu. A. 1989 Do internal solitons exist in the ocean? *Rev. Geophys.* **27**, 293–310.

Sazonov, I. A. & Shrira, V. I. 2003 Quasi-modes in boundary-layer-type flows. Part 2. Large-time asymptotics of broadband inviscid small amplitude two-dimensional perturbations. *J. Fluid Mech.* **488**, 245–288.

Shrira, V. I. 1989 On the 'sub-surface' waves of the mixed layer of the upper ocean *Dokl. Akad. Nauk SSSR* **308**, 732–736. Engl. translation: *Trans. USSR Acad. Sci., Earth Sci.* **308**, 276–279.

Shrira, V. I. & Sazonov, I. A. 2001 Quasi-modes in boundary-layer-type flows. Part 1. Inviscid two-dimensional spatially harmonic perturbations. *J. Fluid Mech.* **446**, 133–171.

Shrira, V. I., Voronovich, V. V. & Sazonov, I. A. 2000 Wave breaking due to internal wave–shear flow resonance over a sloping bottom. *J. Fluid Mech.* **425**, 187–211.

de Sterke, C. M., & Sipe, J. E. 1994 Gap solitons. *Prog. Opt.* **33**, 203–2221.

Voronovich, V. V., Pelinovsky, D. E. & Shrira, V. I. 1998*a* On internal wave – shear flow resonance in shallow water. *J. Fluid Mech.* **354**, 209–237.

Voronovich, V. V. & Shrira, V. I. 1996 On the amplification of internal-wave surface manifestations due to subsurface shear current. *Oceanology* **36**, 157–161.

Voronovich, V. V., Shrira, V. I. & Stepanyants, Yu. A. 1998*b* Two-dimensional models for nonlinear vorticity waves in shear flows. *Stud. Appl. Maths* **100**, 1–32.